AIAA SciTech Forum
6-10 January 2020, Orlando, FL
AIAA Scitech 2020 Forum

10.2514/6.2020-2046

Computational Study of Flapping Wing Response to Vertical Gusts at Low Reynolds Numbers

Naresh Poudel[1], Lai Wang[2], and Meilin Yu[3]
University of Maryland, Baltimore County, Baltimore, MD, 21250, USA

and
John T Hrynuk[4]
Combat Capabilities Development Command - Army Research Lab, Aberdeen Proving Ground, MD, 21005, USA

This work presents a computational study of an oscillating NACA0012 airfoil's response to vertical gusts at low Reynolds numbers. The gust is created by a cross-flow ducted floor jet and its interaction with a freestream flow causes the jet to bend downstream, thus creating a blockage effect and modifying the effective angle of attack (AoA) over an airfoil in the freestream flow. The interaction of the gust with the airfoil causes large unsteady forces, which exceed the peak static lift coefficient. As the gust becomes fully developed near the airfoil region, the airfoil exhibits a leading edge vortex formation and dynamic-stall-like phenomenon while remaining at a fixed zero degree AoA. The gust-wing interactions under dynamic pitching conditions are also studied by varying the reduced frequencies. The study shows that the effects of the gust can be mitigated by increasing the reducing frequency of the flapping wing. As a byproduct, larger lift and thrust will be produced.

I. Nomenclature

Re	=	Reynolds Number
c	=	chord length
t	=	time
Δt	=	time step
t*	=	convective time
U_∞	=	freestream velocity
V_g	=	gust velocity
A	=	pitching amplitude
θ_m	=	mean angle of attack
θ_0	=	amplitude of the pitching angle
f	=	oscillation frequency
S_t	=	Strouhal Number
k	=	reduced frequency
$\emptyset$	=	phase difference

[1] Graduate Student, Department of Mechanical Engineering, and AIAA Student Member. Email: npoudel1@umbc.edu.
[2] Graduate Student, Department of Mechanical Engineering, and AIAA Student Member. Email: bx58858@umbc.edu.
[3] Assistant Professor, Department of Mechanical Engineering, and AIAA Senior Member. Email: mlyu@umbc.edu.
[4] Mechanical Research Engineer, Vehicle Technology Directorate, CCDC Army Research Lab.

II. Introduction

Due to their small size and low speed, Micro Air Vehicles (MAVs) are prone to encounter flight maneuverability and control issues due to ambient unsteady flow environments, such as wind gusts. These unsteady loads due to cross-wind and vertical gusts play a significant role in the design and operation of MAVs. Early in aviation history gust research focused primarily on the response of large aircraft[1], but these tests seldom reflected the aerodynamic conditions experienced by MAVs. Due to the gusty wind conditions in low atmospheric urban areas and the relative speed of the vehicle, MAVs may experience large changes in AoA. Therefore, the impact of gust response on the aerodynamic performance and structure of MAVs should be understood for all extreme cases in order to better design future promising MAVs. Flying birds and insects provide examples of vehicles that can alleviate the adverse effects of unsteady ambient flow. Some of this may be due to their inherent aerodynamic capability of the flapping wing mechanism. However, most studies for the flapping motion of the birds and insects have neglected the effect of wind gust on the stability of the motion[2]. This study will establish a fundamental understanding of the hidden flow physics underlying the fluid dynamics of flapping wings interacting with gust.

Current understanding of gusts is usually limited by the methods that researchers have used to develop vertical gusts in an experimental setting. While computational fluid dynamics (CFD) studies of gust interactions are not uncommon[3-5], they are seldom thoroughly compared to experimental results under different gusty conditions; and results on gust mitigation with flapping wings are limited. In our recent studies[6-8], a comparison of gust wing interaction simulated experimentally with a vertical gust generator in a wind tunnel environment and numerically with advanced unsteady CFD tools has been carried out. Experimental results from Smith *et al.*[7,8] are used to develop inlet and boundary conditions of a CFD model of the experimental setup[8]. This CFD model has been used to further explore extremely time-consuming experimental variables, such as turbulence reduction, and widen the understanding of mechanism of gust generation in a wind tunnel.

III. Background

Study of the fundamental response of MAV-scale vehicles to vertical gusts is key to the development of active and passive gust rejection methods for future MAVs. Past studies have usually focused on small amplitude transient vertical gusts, where a small change in wing AoA (α) was modeled as a transient lift effect. These methods include Wagner's indicial function and Kussner's function for estimating the lift changes as a function of gust encounter under the assumptions of low gust ratios, inviscid and attached flow conditions. However, recent work by Smith[6] has shown that a vertical gust encounter in a wind tunnel environment bears little resemblance to the flow conditions of a static wing. This result suggested that linear theories are unlikely to properly represent gust encounters.

Other methods have previously been used for the study of vertical gust encounters. Traditionally a diffuse vortex generated upstream of test models was used to simulate vertical gust interactions (Patel and Hancock[9], Buell[10]). While the generated vortex diffused before hitting the model, the method provides only transient up and downdraft behavior. Another common gust generating method is to actuate a wing under gust like maneuvers, i.e. plunging wings, in a water tunnel or towing tank (Baik *et al.* [11]; Perrotta *et al.*[12]). These methods have been shown to be effective for the study of gust interactions, but each has unique challenges. Plunging wings have high potential to mimic some gust-like behaviors, but it remains unknown the extent of the

differences between moving-body and moving-fluid gust interactions. Towing tank studies like Perrotta *et al.*[12] produce high quality results but were limited in their transient nature, where the wing must keep moving and pass through the gust. This limited their ability to create a step-function-like gust, which would simulate a MAV flying into an updraft wider than the vehicle itself. The numerical studies over the pitching airfoil in unsteady flow environments significantly affect the aerodynamic performance of the flapping wing by modifying the vortex structures[13]. High-order CFD methods had been proven more accurate and efficient to capture the complex vortex-dominated flow structures due to flapping wings[14]. In this study, we use a high-order CFD solver to investigate the gust mitigation performance of oscillating airfoils.

IV. Numerical Methods

Governing Equations

Unsteady compressible Navier-Stokes equations in conservation form are considered in the physical domain (t, x, y) as follows:

$$\frac{\partial Q}{\partial t} + \frac{\partial F}{\partial x} + \frac{\partial G}{\partial y} = 0, \tag{1}$$

where $Q = (\rho, \rho u, \rho v, E)^T$ are conserved variables, ρ is the density of fluid, , u and v are the x- and y-components of the velocity and E is the total energy given by $E = \frac{p}{\gamma - 1} + \frac{1}{2}\rho(u^2 + v^2)$ for a perfect gas in which p is the pressure and γ is the constant specific heat capacity ratio. The total energy formula closes the solution system. F and G are total flux vectors including the inviscid and viscous flux terms in the x- and y-direction, respectively. To facilitate numerical simulation, the governing equation (1) in the physical domain (t, x, y) is transformed into computational domain (τ, ξ, η) as shown in Eq. (2). In the coordinate transformation, $\tau = t$ and $(\xi, \eta) \in [-1, 1] \times [-1, 1]$ is a standard element in the computational domain.

$$\frac{\partial \tilde{Q}}{\partial \tau} + \frac{\partial \tilde{F}}{\partial \xi} + \frac{\partial \tilde{G}}{\partial \eta} = 0, \tag{2}$$

where

$$\begin{cases} \tilde{Q} = |J|Q \\ \tilde{F} = |J|(Q\xi_\tau + F\xi_x + G\xi_y) \\ \tilde{G} = |J|(Q\eta_\tau + F\eta_x + G\eta_y) \end{cases}. \tag{3}$$

The Jacobian matrix of the coordinate transformation can be written as the following form:

$$J = \frac{\partial(x, y, t)}{\partial(\xi, \eta, \tau)} = \begin{pmatrix} x_\xi & x_\eta & x_\tau \\ y_\xi & y_\eta & y_\tau \\ 0 & 0 & 1 \end{pmatrix}. \tag{4}$$

The inverse transformation must also exist for a non-singularity transformation, which can be related to the Jacobian matrix as:

$$J^{-1} = \frac{\partial(\xi, \eta, \tau)}{\partial(x, y, t)} = \begin{pmatrix} \xi_x & \xi_y & \xi_t \\ \eta_x & \eta_y & \eta_t \\ 0 & 0 & 1 \end{pmatrix}. \tag{5}$$

Spatial Discretization and Time Integration Methods

The flux reconstruction/correction procedure via reconstruction (FR/CPR)[15-22] method is used to solve the governing equations. A brief introduction of FR/CPR method is discussed in this section for the sake of completeness. In FR/CPR methods, the flux terms in Eq. (2) are divided into two parts, i.e. local fluxes constructed from local solutions and correction fluxes by mapping the differences between the local fluxes and the common fluxes on the element interfaces to the entire element. This can be expressed as:

$$\begin{cases} \tilde{F}(\xi,\eta) = \tilde{F}^{loc}(\xi,\eta) + \tilde{F}^{cor}(\xi,\eta) \\ \tilde{G}(\xi,\eta) = \tilde{G}^{loc}(\xi,\eta) + \tilde{G}^{cor}(\xi,\eta) \end{cases}. \tag{6}$$

On substituting Eq. (6) into Eq. (2), the governing equations can be reformulated as:

$$\frac{\partial \tilde{Q}}{\partial \tau} + \left(\frac{\partial \tilde{F}^{loc}}{\partial \xi} + \frac{\partial \tilde{G}^{loc}}{\partial \eta}\right) + \left(\frac{\partial \tilde{F}^{cor}}{\partial \xi} + \frac{\partial \tilde{G}^{cor}}{\partial \eta}\right) = 0, \tag{7}$$

In this study, the inviscid common fluxes at the cell interfaces are calculated using the Roe approximate Riemann Solver[23] and the common viscous fluxes at the cell interfaces were obtained by the approach developed by Bassi and Rebay[24].

Equation (1) can be written as

$$\frac{\partial Q}{\partial t} = R(Q), \tag{8}$$

The explicit first stage, singly diagonally implicit Runge-Kutta (ESDIRK) method[20, 21] is used for time integration, which is written as

$$\begin{cases} Q^{n+1} = Q^n + \Delta t \sum_{i=1}^{s} b_i R(Q_i) \\ Q_i = Q^n + \Delta t \sum_{j=1}^{i} a_{ij} R(Q_j), \qquad i = 1, \dots s, \end{cases}. \tag{9}$$

where s is the number of stages and

$$a_{ii} = \begin{cases} 0, i = 1, \\ \omega, i \neq 1. \end{cases} \tag{10}$$

Equation (9) can be written as

$$\begin{cases} Q^{n+1} = Q^n + \Delta t \sum_{i=1}^{s} b_i R(Q_i), \\ Q_1 = Q^n, \\ Q_i = \Delta t \omega R(Q_i) + Q^n + \Delta t \sum_{j=1}^{i-1} a_{ij} R(Q_j), \qquad i = 2, \dots s, \end{cases}. \tag{11}$$

In this study, the second-order, three-stage ESDIRK2 with the time step of 10^{-2} was used. The radial basic function from earlier work[22] is used for dynamic mesh deformation to interpolate the mesh to different stages. We use Lagrange polynomials of the coordinates at different stages to compute the grid velocities. The geometric conservation law was enforced in order to eliminate the grid motion induced errors.

V. Verification and Validation (V&V) of the CFD Solver

The V&V of the flow solver was done under uniform flow conditions. Numerical results are compared with the published data from previous experiments and computations. Table 1 shows comparison of drag coefficient (C_D) at Reynolds number (Re) 12,000 at zero AoA under uniform flow conditions. The current drag coefficient agrees well with the reference data[25-28].

Source	C_D
Current	0.0347
Hammer *et al.*[25]	0.0350
Laitone[26]	0.0334
Liu and Kawachi[27]	0.0346
Young and Lai[28]	0.0361

Table 1: Comparison of C_D for NACA 0012 at Re = 12,000 and AoA = 0^0 in a uniform flow.

VI. Airfoil Kinematics and Computational Domain

In this study, the NACA0012 airfoil is undergoing pitching motion, which is expressed as:

$$\theta(t) = \theta_m + \theta_0 \sin(2\pi f t + \emptyset) \ , \qquad \textbf{(12)}$$

where θ_m is the mean angle of attack, θ_0 is the amplitude of the pitching angle, $\emptyset$ is the initial phase, f is the oscillating frequency, t is the dimensional time and h_0 is the non dimensional plunging amplitude. The reduced frequency, k and Strouhal number, S_t are given as:

$$k = \frac{\pi f c}{U_\infty}$$
$$S_t = \frac{2fA}{U_\infty} \ , \qquad \textbf{(13)}$$

where c is the chord length of the airfoil, A is the pitching amplitude and U_∞ is the freestream velocity.

Figure 1 shows the computational domain used for the numerical study of gust-wing interaction. The dimensions of the computational domain were calculated to match those from the wind tunnel experiment[7, 8]. For this simulation, a far field boundary was used for the top of the computational domain, which is different from the top wall of the wind tunnel. However, preliminary results[6] showed that this had no effect when compared to the wind tunnel testing. Fixed inlet and outlet boundaries and a symmetry boundary on the bottom of the computational domain were enforced in the simulation. For the gust inlet, vertical gust velocity similar to experimental setup was given. The gust ratio (GR) is defined as the vertical speed of gust divided by the freestream flow $\left(\frac{V}{U_\infty}\right)$.

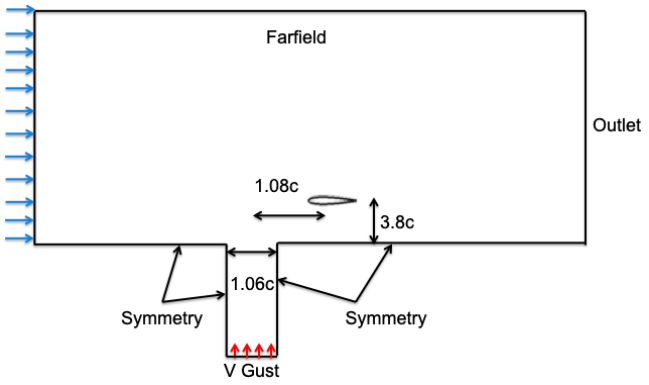

Figure 1: An illustration of the computational domain.

VII. Results and Discussions

Gust-Wing Interaction over a Stationary Airfoil

In the numerical study of the gust-wing interaction at zero AoA and Reynolds number 12,000, the simulation was first conducted without the gust to develop the flow over the airfoil. After running the simulation for about 32 non-dimensionalized time ($t^*=tU_\infty/c$, where U_∞ is the free stream velocity, and c is the chord length of the airfoil), the gust was turned on. Figure 2 shows the drag and lift coefficient histories on the NACA 0012 airfoil. It can be seen that when the gust is off, the drag and lift coefficients (C_D and C_L) are close to those under the uniform flow condition. After the gust is turned on, the gust-wing interaction can be characterized by dividing it into four stages as shown in Figure 2. Each stage is described as follows.

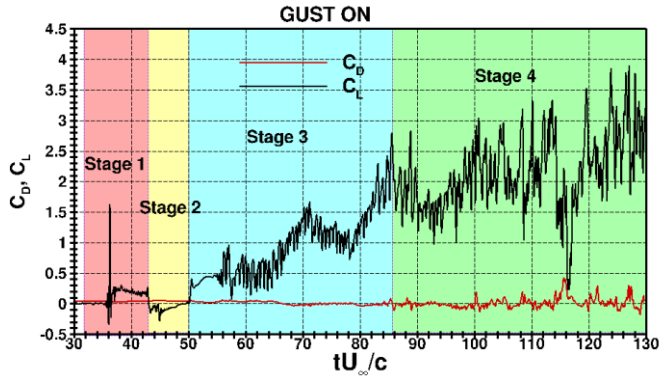

Figure 2: Histories of drag and lift coefficients for NACA 0012 at Re = 12,000 and AoA = 0^0 with gust.

Stage 1:

Once the gust is turned on, it took around $t^*= 3.5$ to be fully developed in the gust inlet. When the gust reached the upper portion of the gust inlet, the airfoil experiences the sudden pressure wave propagation from gust, resulting in a sudden spike in the lift coefficient. As the gust starts to develop, the lift coefficient increases gradually until $t^* = 43$.

Stage 2:

In Stage 2, there is a sudden decrease in the lift coefficient due to the low-pressure regions developed beneath the airfoil. No leading edge vortices are developed in this stage.

Stage 3:

In Stage 3, the gust starts to gradually change the AoA of the airfoil, and the lift coefficient increases until the gust is fully developed. After t* = 50, the gust starts to interact with the airfoil, and the shear layer from the lower surface of the airfoil begins to bend towards the leading edge of the suction side of the airfoil. At t* = 55.3, as the interaction of gust progresses, the separation bubble near the trailing edge grows, causing the flow to separate from the trailing edge of the airfoil, and flow disturbances to advance toward the leading edge. After t* = 55.3, the vortices start to form from the top surface and detach from the airfoil, forming vortex shedding as shown in Figure 3. These leading edge vortices generate a low-pressure region on the top surface of the airfoil, enhancing the lift.

Stage 4:

Once the gust is fully developed, the airfoil experiences a dynamic stall event as the loss and gain in the lift coefficients are observed in the lift coefficient history. At t* = 116.5, the sudden drop in the lift coefficient was observed in Figure 2. This is due to the separation of a large vortex on the top surface of the airfoil, which results in high pressure near the trailing edge as shown in Figure 4. When leading edge vortices are formed again and the large vortex passes away to the wake region, the lift coefficient is recovered.

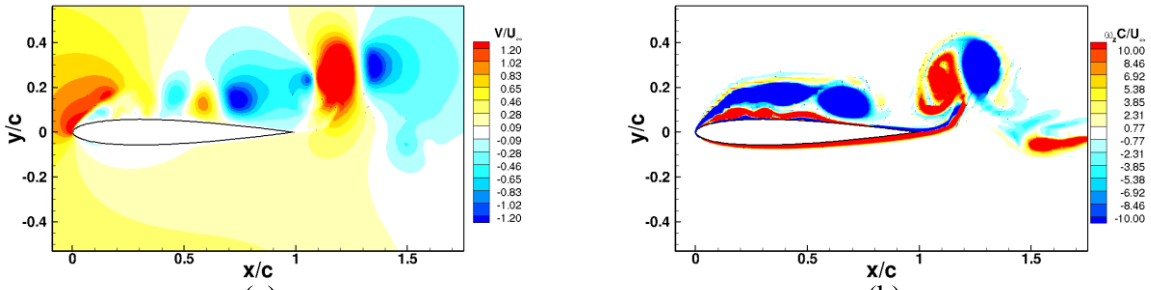

(a) (b)

Figure 3: (a) Gust ratio $\frac{V}{U_\infty}$ $at\ t^* = 85.5$; and (b) an instantaneous vorticity field at t* = 85.5 at Re=12,000.

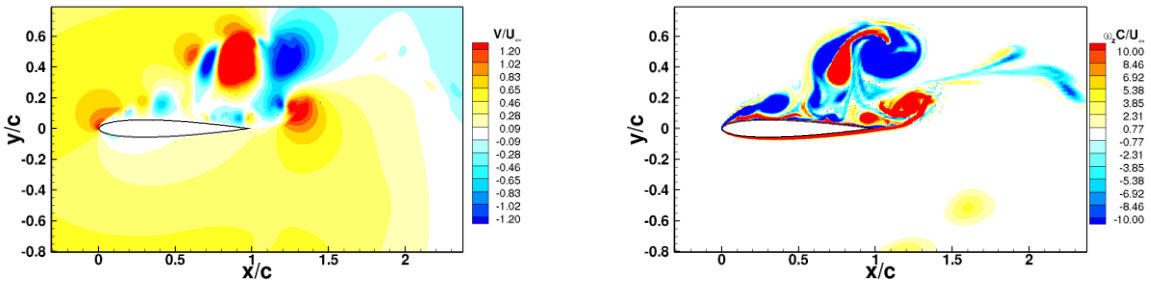

(a) (b)

Figure 4: (a) Gust ratio $\frac{V}{U_\infty}$ $at\ t^* = 116.5$; and (b) an instantaneous vorticity field at t* = 116.5 at Re=12,000.

Gust-Wing Interaction over a Pitching Airfoil

The gust-static wing section showed a wing undergoing a highly unsteady stall event due to the change in effective angle of attack caused by the gust. In this section, the gust-wing interaction

using a flapping wing is presented. Reduced frequency (k) was varied to determine the influence of reduced frequency on the vertical gust response of the wing.

In this study, we considered three reduced frequency cases, shown in Table 2. These changes in reduced frequency also changed the Strouhal number because pitching amplitude was fixed at 10 degrees. For all the three cases, the Reynolds number and the gust ratio $\frac{V}{U_\infty}$ are 12,000 and 0.42, respectively, to match the stationary case which was previously compared to experimental results[5].

Table 2: Pitching airfoil cases

Case	Reduced Frequencies	Strouhal Numbers
1	0.5	0.04
2	1.0	0.08
3	3.93	0.30

To understand the impact of gust-wing interaction over the pitching airfoil, we first analyze the flow fields and force histories over the pitching airfoil before the gust starts to interact (stage 1), and then compare the results after the gust starts to interact with the airfoil (stage 4). Figures 5, 6 and 7 show the instantaneous vorticity fields for one pitching cycle for the three cases shown in Table 2 during the initial gust interaction with the pitching airfoil. T is defined as an oscillation time period for pitching motion airfoil. The red circles on the force history plots show the position of airfoil corresponding to t = 0, t = ¼ T, t= ½ T, t = ¾ T and t = T; and the instantaneous vorticity and gust ratio fields at that instant are presented.

In Figure 5, the airfoil is oscillating with the reduced frequency of k = 0.5. During the early interaction of the gust with the wing (stage 1), the gust ratio is low but the lift was still already effected during the pitch-down motion. In this case a Leading Edge Vortex (LEV) was formed on the suction side of the airfoil which then detached from the trailing edge of the airfoil. Even in the early stage of the gust development, the vortex shedding in the wakes are deflected during different phases of the pitching cycle.

Figure 6 shows the flow phenomena for the stage 1 during the early gust wing interaction for the airfoil pitching with the reduced frequency k = 1. We can observe the different wake pattern compared to the case with the reduced frequency k = 0.5. A stronger LEV is formed for the higher reduced frequency and the lift profile became more symmetric when compared to the lower reduced frequency. This case also exhibited stronger shed vortices that were displaced further above and below the wing.

Figure 7 shows the case when the airfoil is oscillating at the reduced frequency, k = 3.93. Here the vortex shedding pattern from the airfoil is similar to that of an airfoil pitching at this reduced frequency in a uniform flow condition. At this early stage of the gust development, the rapidly pitching airfoil does not experience significant impact from the gust. Smaller LEVs are formed on the suction side of the airfoil compared to the cases with lower reduced frequencies. In this case the reduced frequency is high enough to form the reverse von Karman street indicating a switch to thrusting behavior. In general, the wake for this case is generally not effected by the gust during early gust formation time (stage 1).

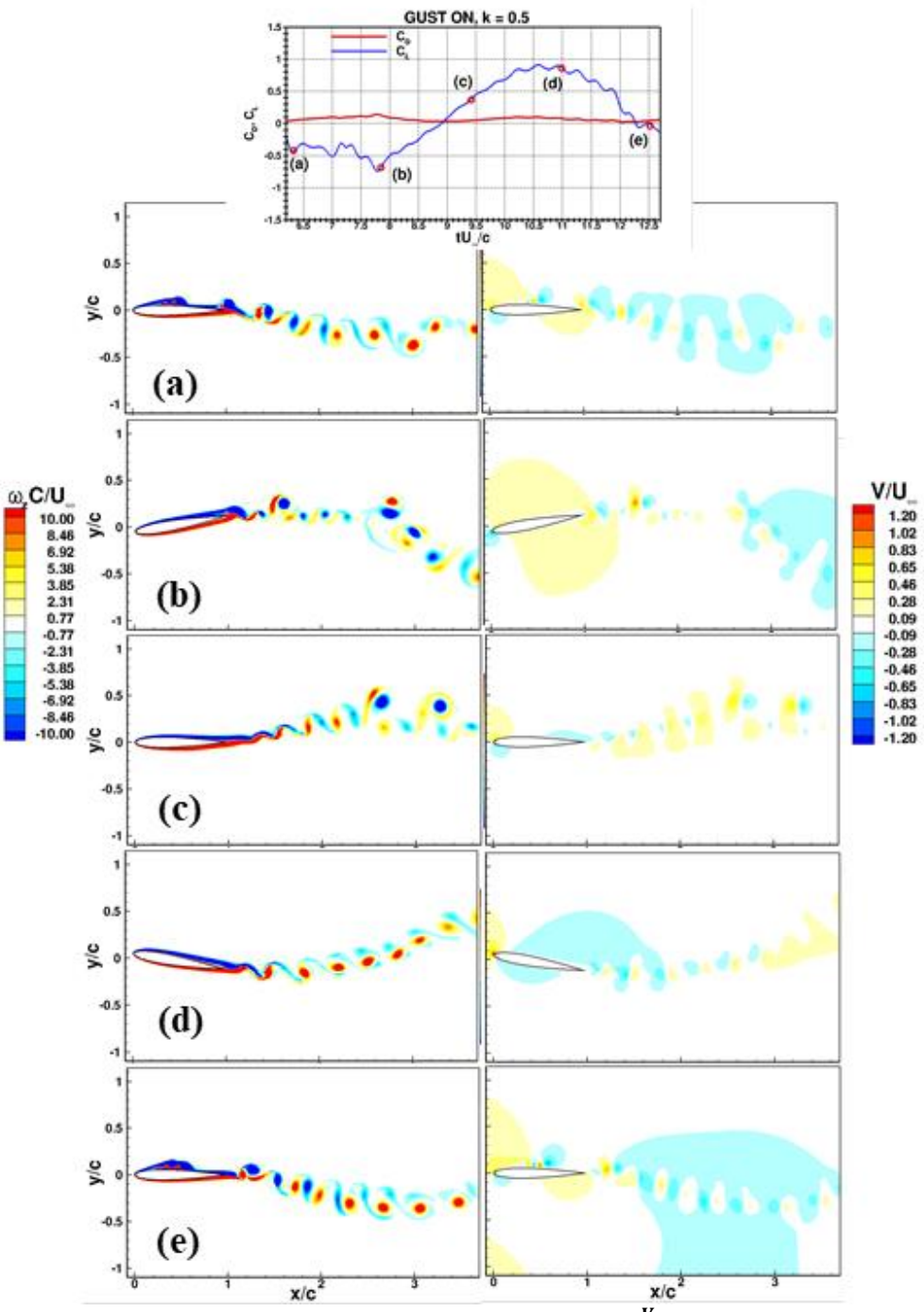

Figure 5: Instantaneous vorticity fields; and Gust ratio $\frac{V}{U_\infty}$ at the stage 1 for k = 0.5.

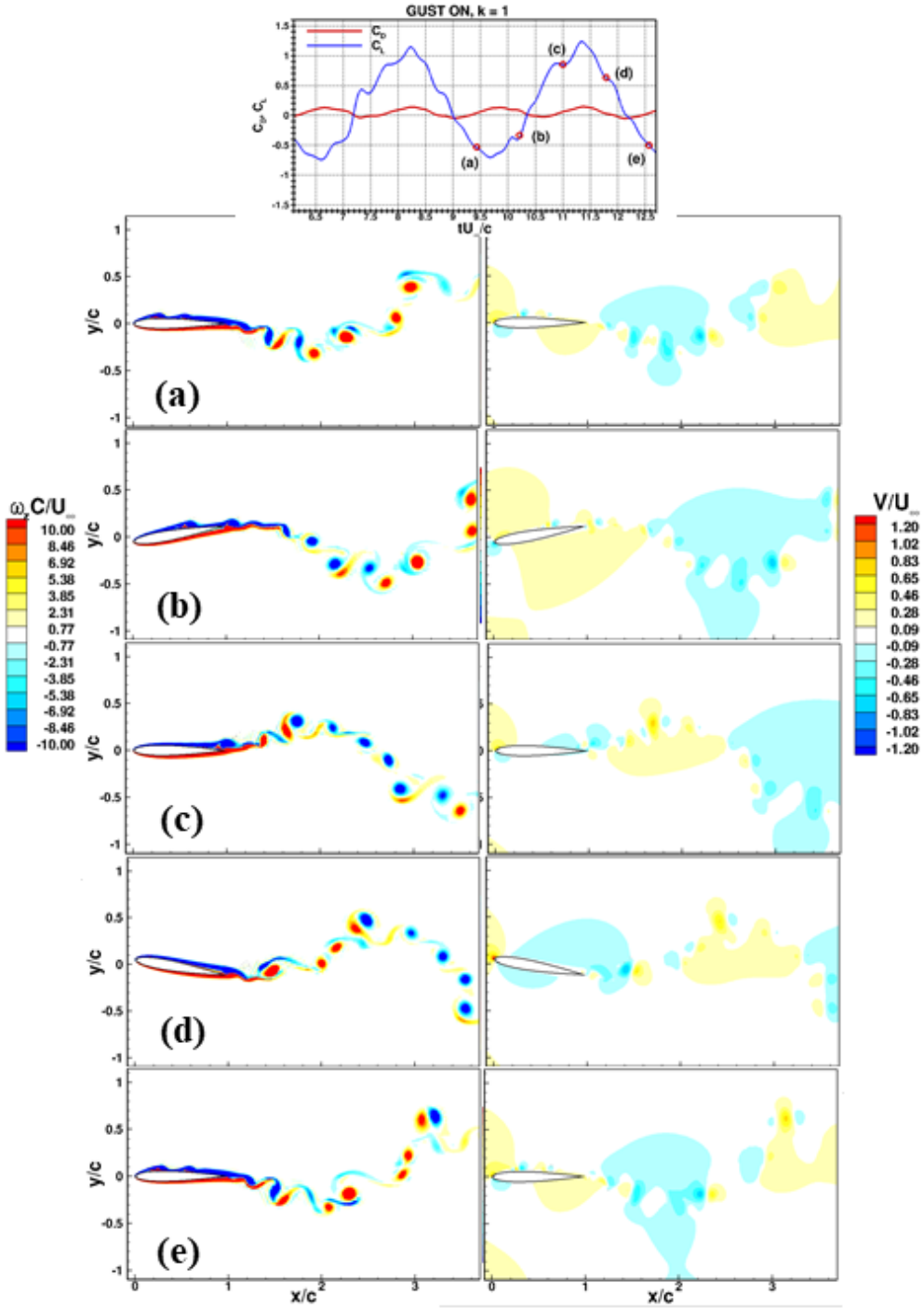

Figure 6: Instantaneous vorticity fields; and Gust ratio $\frac{V}{U_\infty}$ at the stage 1 for k = 1.0.

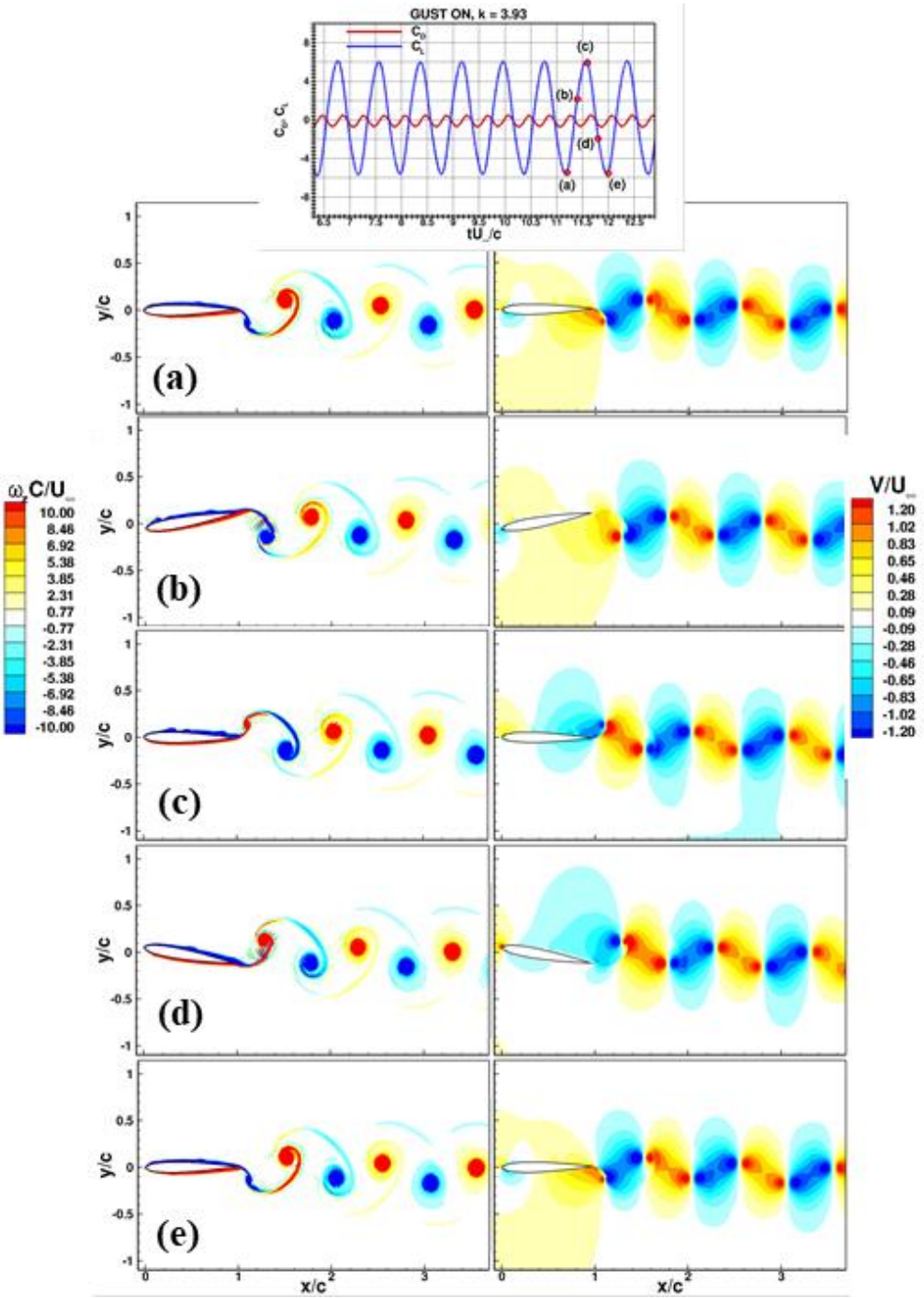

Figure 7: Instantaneous vorticity fields; and Gust ratio $\frac{V}{U_\infty}$ at the stage 1 for k = 3.93

Figures 8, 9 and 10 show flow field visualization for one pitching cycle for the three cases with respect to pitching airfoil at different reduced frequencies after the gust is fully developed (Stage 4). From Figure 8, we can see that the gust ratio near the airfoil reached around $\frac{V}{U_\infty} = 0.46$ changing the effective AoA of incoming flow to approximately 25º over the airfoil due to the vertical gust. Compared to earlier in the gust interaction larger LEVs were formed but the lift behavior was still

significantly affected by the gust, which introduced unsteadiness into the usual sinusoidal lift behavior.

For the case with the reduced frequency of k = 1, more large LEVs are formed compared to the lower pitch rate case. The flow field became significantly more complex and that was reflected in the lift behavior. At this point the lift curve bears little resemblance to the usual sinusoidal behavior.

When the airfoil is pitching at the reduced frequency of k = 3.93, Figure 10, the LEVs were smaller than the lower reduced frequencies at the same stage of gust development. At this higher pitching frequency the gust effect was generally suppressed and the overall lift and thrust coefficients are increased compared to a uniform free-stream case. The wakes are also deflected downward for each phase of pitching cycle. At the reduced frequency k = 3.93, we observe that the flow evolves slowly and remains attached to the airfoil even after the gust interacts with the airfoil and the vortex shedding structures are more organized than the lower reduced frequency cases. In general, this data suggests the high reduced frequency pitching dominates the flow. This was in spite of the incoming flow condition generating a highly unsteady stall for a fixed angle case. Note that the average lift here exceeds the static stall lift for a NACA 0012 under these conditions.

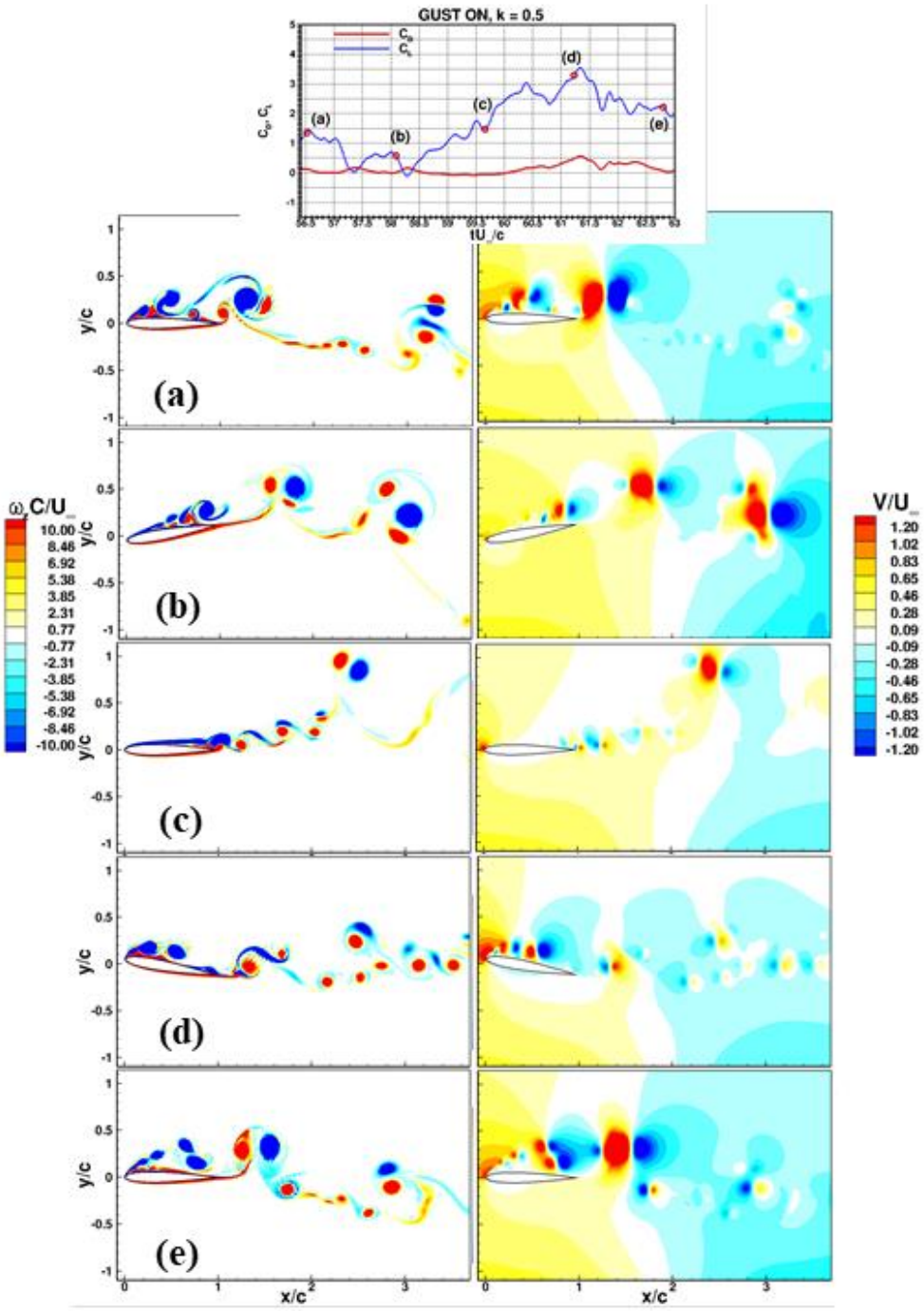

Figure 8: Instantaneous vorticity fields; and Gust ratio $\frac{V}{U_\infty}$ at the stage 4 for k = 0.5.

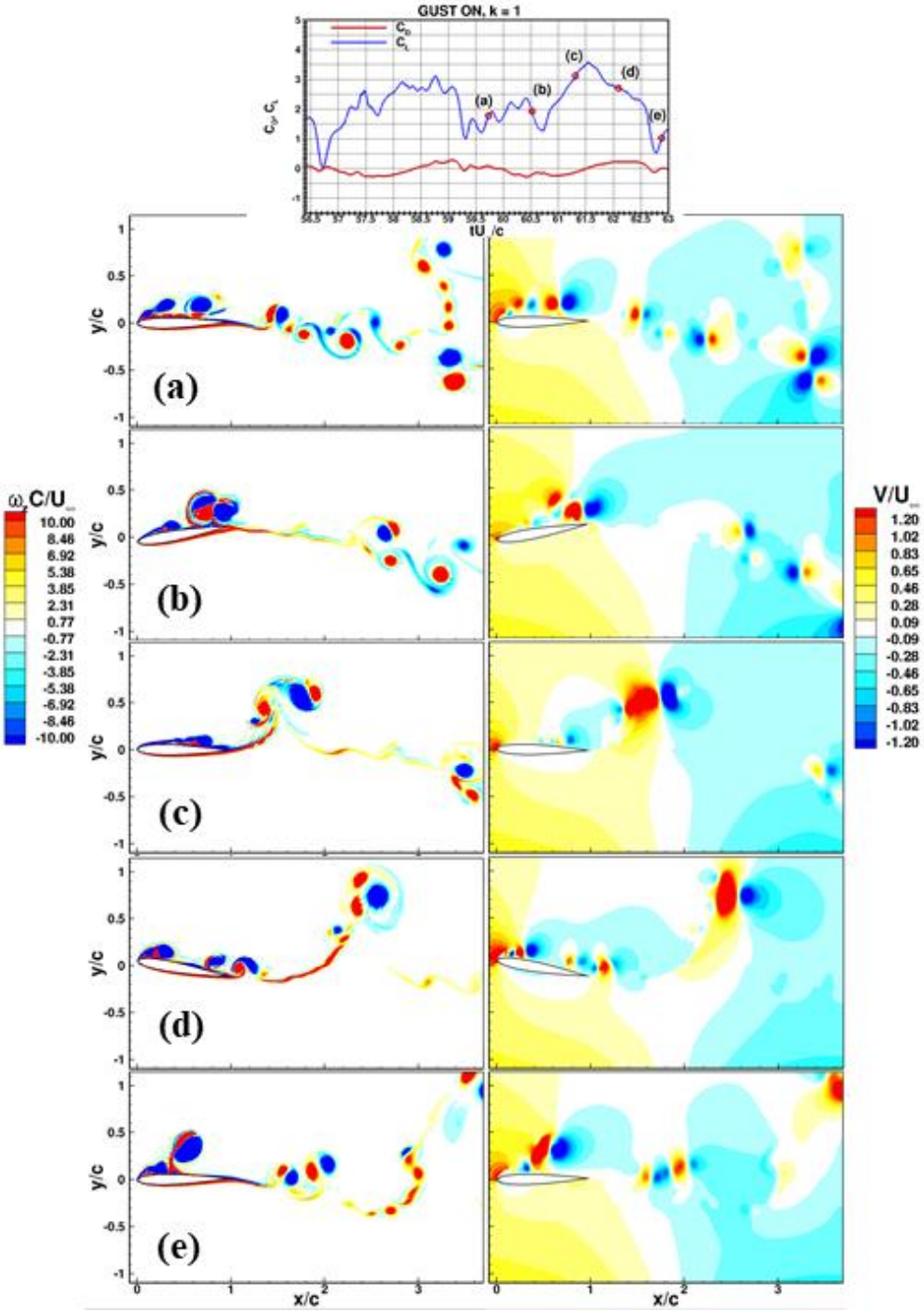

Figure 9: Instantaneous vorticity fields; and Gust ratio $\frac{V}{U_\infty}$ at the stage 4 for k = 1.0

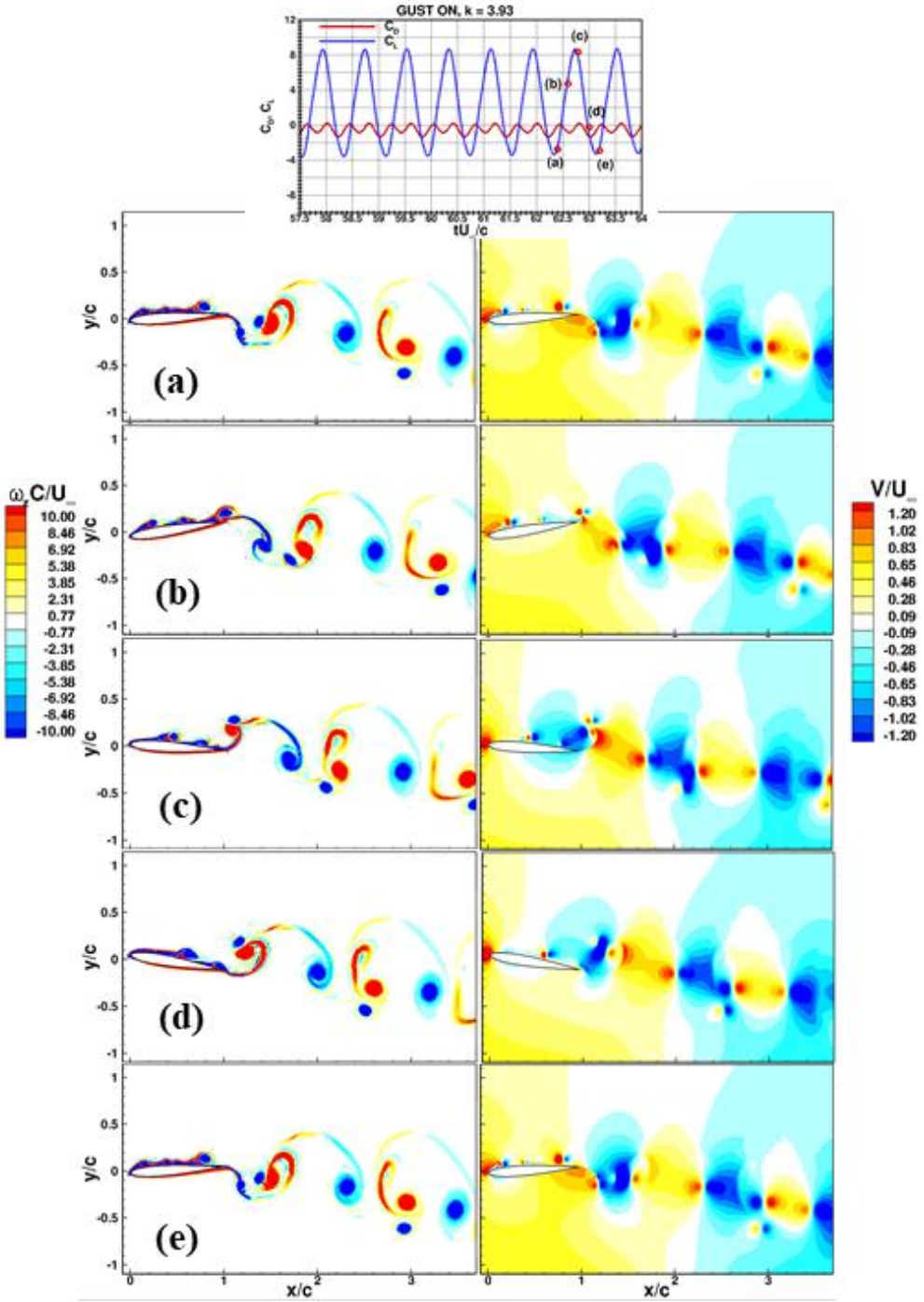

Figure 10: Instantaneous vorticity fields; and Gust ratio $\frac{V}{U_\infty}$ at the stage 4 for k = 3.93

Aerodynamic Forces Analysis

Looking at the aerodynamic forces over time provides a clearer picture of the gust effects on lift and drag/thrust. The gust alters the incoming flow angle beyond the static stall angle but at a slower rate than the reduced frequency of the pitching motion. The forces acting on the airfoil are

decomposed into horizontal (drag, thrust) and vertical (lift) directions with respect to the position of airfoil. The drag and lift coefficients are

$$C_D = \frac{2F_X}{\rho U_\infty^2 A}, \qquad C_L = \frac{2F_Y}{\rho U_\infty^2 A}, \tag{14}$$

where F_X is the drag force, F_Y is the lift force, ρ is the fluid density, U_∞ is the freestream velocity and A is the area.

Figure 11 (a) and (b) show the drag and lift coefficients histories for the pitching airfoil at two reduced frequencies k = 0.5 and k = 1, compared with those for the stationary airfoil. The mean lift trends (C_L) are similar for the low reduced frequency cases and the stationary wing. Early on the gust had a limited effect on the mean and oscillating lift. Later as the gust grew in magnitude the unsteadiness of both the stationary and low reduced frequency cases grew as a function of time.

Figure 11 (c) and (d) show the drag and lift coefficients histories for the airfoil pitching at a higher reduced frequency k = 3.93, compared with those for the stationary airfoil. For the higher reduced frequency the force histories are quite periodic and fluctuations observed at lower reduced frequencies are not seen. Mean lift for this case rises in the same fashion as the stationary airfoil cases but the time scale for the higher reduced frequency appears to mitigate the unsteadiness caused by the gust. The wing maintains its thrusting behavior despite the large effects of the gust observed for lower reduced frequencies. These results further the supposition that high reduced frequency pitching behaviors dominate the flow compared to large amplitude gusts at slower time-scales.

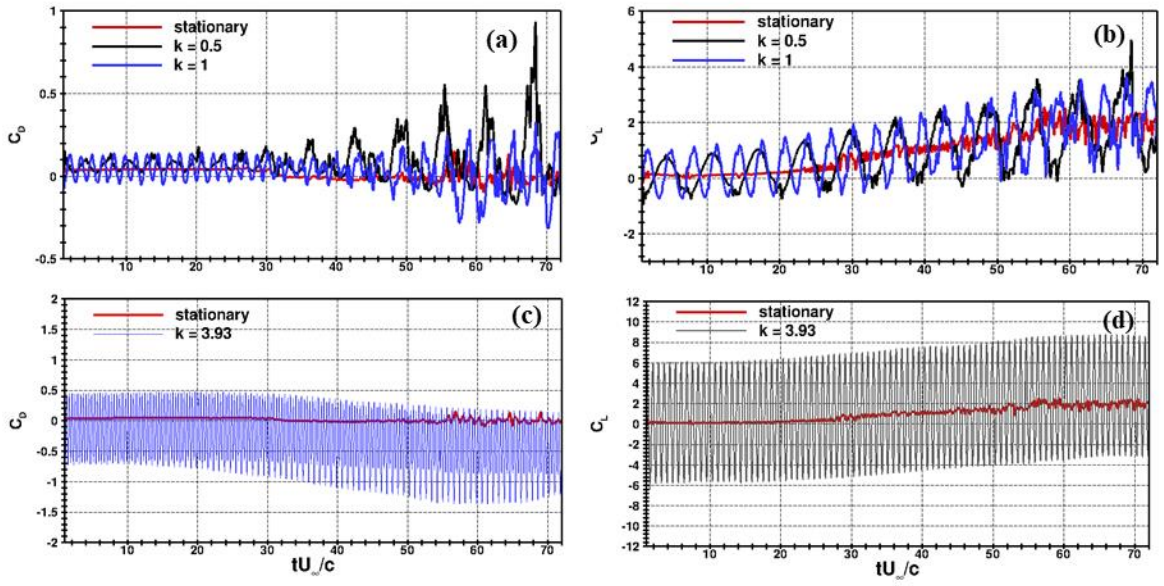

Figure 11: Drag and Lift coefficients histories

Figure 12 shows the time averages of the aerodynamic force coefficients on the airfoil for the stationary airfoil, oscillating airfoil at reduced frequencies 0.5, 1 and 3.93 during the early gust development stage (stage 1) and after gust interaction stage (stage 4). During the stage 4, the drag

changed to thrust due to gust interaction for cases with k = 1 and k = 3.93 as shown in Figure 12(a). For the case with k =3.93, the gust interaction at stage 4 increases the thrust twice as much as stage 1.

At stage 1 for the oscillating airfoil, the gust shifts the average lift coefficients (C_L) slightly up compared to the static airfoil. The gust causes C_L at k = 0.5 to be lower than the static wing likely due to the unsteadiness form the gust. The average C_L for the cases with k =1 and k = 3.93 are increased due to gust at stage 4 compared to the static wing as shown in Figure 12 (b).

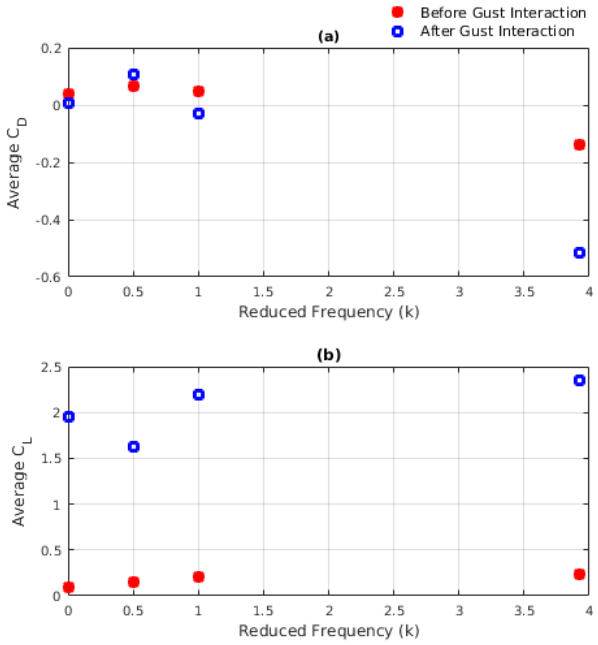

Figure 12: Time averaged aerodynamics forces before and after gust-wing interaction. (a) Drag coefficient and (b) lift coefficient for stationary airfoil, pitching airfoil at reduced frequencies 0.5, 1 and 3.93.

VIII. Conclusion and Future Work

The gust-wing interaction with a stationary NACA0012 airfoil at zero AoA has been compared with several pitching cases with different reduced frequencies. The stationary airfoil undergoes a highly unsteady stall process at zero degree AoA when vertical gusts are applied. The lift coefficient increased as the gust grows but became highly unsteady after stalling. However, the mean lift in the post-stall region exceeded the peak static lift coefficient despite the unsteady behavior. Pitching the airfoil had several different effects. At low reduced frequencies the gust dominated the flow field causing a highly unsteady influence on the typically sinusoidal lift curves of pitching airfoils. Pitching at the higher reduced frequency overcomes the flow disturbances caused by vertical gusts, but the gust significantly increased both the lift and thrust. In the case of thrust, the thrust of the airfoil pitching at high reduced frequency (k = 3.93) was more than doubled by the gust interaction. Future work will include the evaluation of the source of the increased thrust associated with the gust, specifically focused on determining if this effect is caused by the gust generation method or is inherent to gust-pitching wing interactions.

Acknowledgements

Research was partially supported by the Combat Capabilities Development Command - Army Research Laboratory under CRADA 14-054-003. The views and conclusions in this document are those of the authors and should not be interpreted as representing the official policies, either expressed or implied, of the Army Research Laboratory or the U.S. Government. The U.S. Government is authorized to reproduce and distribute reprints for Government purposes notwithstanding any copyright notation herein. The hardware used in the computational studies is part of the UMBC High Performance Computing Facility (HPCF). The facility is supported by the U.S. National Science Foundation through the MRI program (grant nos. CNS-0821258, CNS-1228778, and OAC-1726023) and the SCREMS program (grant no. DMS-0821311), with additional substantial support from the University of Maryland, Baltimore County (UMBC).

References

[1] Donely, P., Summary of Information Relating to Gust Loads on Airplanes, NACA Report 997, 1950.

[2] Shyy, W., Aono, H., Chimakurthi, S.,K., Trizila , P., Kang, C.-K., Cesnik, C.E., Liu, H., *Recent progress in flapping wing aerodynamics and aeroelasticity,* Prog. Aerosp. Sci., 46 (7) (2010), pp. 284-327.

[3] Xu, X.P., Zhu, X.P., Zhou, Z., Chang, M., *Numerical Simulation of Gust Response for UAV Airfoil,* Proceedings of the 2010 Asia-Pacific International Symposium on Aerospace Technology, Vol 1 and 2, pp. 403, 2010.

[4] Liauzun, C., Aeroelastic Response to Gust Using CFD Techniques, Proceedings of the ASME Fluids Engineering Summer Meeting, pp. 269-276, 2010.

[5] An, J.G., Yan, Z., Qiu, C.R., Zhou, W.B., The Numerical Computation of Aircraft Response to Arbitrary Vertical Gust Distributions, Journal of Aircraft, Vol. 22 (11), pp. 988-992, 1985.

[6] Poudel, N., Smith, Z., Yu, M., Hrynuk, J.T., *A combined experimental and computational study of a vertical gust generator in a wind tunnel*, AIAA SciTech Forum, 2019-2166.

[7] Smith, Z.F., Jones, A.R., Hrynuk, J.T., Micro Air Vehicle Scale Gust-Wing Interaction in a Wind Tunnel, 2018 AIAA Aerospace Sciences Meeting, AIAA SciTech Forum, 2018-0573.

[8] Smith, Z.F., Micro Air Vehicle Scale Gust-Wing Interaction in a Wind Tunnel, Master of Science Thesis, University of Maryland, College Park, MD, 2018.

[9] Patel, M. H., Hancock, G. J., A gust tunnel facility, Aeronautical Research Council Reports and Memoranda, Reports and memoranda number 3802, June 1976.

[10] Buell, D. A., An experimental investigation of the velocity fluctuations behind oscillating vanes, NASA Technical note NASA TN D-5543, Nov. 1969.

[11] Baik, Y., Bernal L., Granlund K., Ol M., Unsteady force generation and vortex dynamics of pitching and plunging aerofoils, Journal of Fluid Mechanics, Vol. 709, Aug. 2012.

[12] Perrotta G., Jones A., Unsteady forcing on a flat-plate wing in large transverse gusts, Experiments in Fluids 58:101, Aug. 2017.

[13] Poudel, N., Yu, M., *Numerical study of flapping-wing flow physics in nonuniform freestream using high-order spectral difference method on dynamic unstructured grids*, in 2018 Fluid Dynamics Conference, AIAA Aviation Forum, 2018-3087.

[14] Yu, M., L., Wang, Z., J., Hu, H., *A high-order spectral difference method for unstructured dynamic grids*, Computers & Fluids, Vol. 48, pp. 84-97, 2011.

[15] Huynh, H.T., *A flux reconstruction approach to high-order schemes including discontinuous Galerkin methods*, the 18th AIAA Computational Fluid Dynamics Conference, 2007-4079.

[16] Wang, Z., J., Gao, H., Y., *A unifying lifting collocation penalty formulation including the discontinuous Galerkin, spectral volume/difference methods for conservation laws on mixed grids, J. Comput. Phys.,* vol. 228, pp. 8161-8186, 2009.
[17] Vincent, P., E., Castonguay, P., Jameson, A., *A new class of high-order energy stable flux reconstruction schemes*, *J. Sci. Comput.*, vol. 47, pp. 50-72, 2010.
[18] Yu, M., L., Wang, L., *A high-order flux reconstruction/correction procedure via reconstruction formulation for unsteady incompressible flow on unstructured moving grids*, Computers & Fluids, Vol. 139, pp. 161-173, 2016.
[19] Wang, L., Yu, M., L., *On the parallel implementation and performance study of high-order Rosenbrock-type implicit Runge-Kutta methods for the FR/CPR solutions of the Navier-Stokes equations*, AIAA Aerospace Sciences Meeting, 2018, AIAA-2018-1095.
[20] Wang, L., Yu, M., L., *A Comparative study of implicit Jacobian-free Rosenbrock-Wanner, ESDIRK and BDF methods for unsteady flow simulation with high-order flux reconstruction formulations*, submitted.
[21] Wang, L., Yu, M., *Jacobian-free implicit p-adaptive high-order compact direct flux reconstruction methods for unsteady flow simulation,* in 2019 AIAA Aviation Forum, 2019-3062.
[22] Wang, L., Yu, M., *An Implicit High-Order Preconditioned Flux Reconstruction Method for Low-Mach-Number Flow Simulation with Dynamic Meshes*, International Journal for Numerical Methods in Fluids, 2019.
[23] Roe, P.L., *Approximate Riemann solvers, parameter vectors and difference schemes*, Journal of Computational Physics, Vol. 43, pp. 357-372, 1981.
[24] Bassi, F., Rebay, S., A high-order accurate discontinuous finite element method for the numerical solution of the compressible Navier-Stokes eqautions, Journal of Computational Physics, Vol. 131, no. 2, pp. 267-279, 1997.
[25] Hammer, P.R., Visbal, M.R., Naguib, A.M., Koochesfahani, M., *Lift on a steady 2-D symmetric airfoil in viscous uniform shear flow*, J. Fluid Mech, 837, R2, 2018.
[26] Laitone, E., Wind tunnel tests of wings at Reynolds numbers below 70,000, Experiments in Fluids 23, 405-409, 1997.
[27] Lui, H., Kawachi, K., *A numerical study of undulatory swimming*, Journal of Computational Physics, 155, 223-247, 1999.
[28] Young, J., & Lai, J., *Oscillation frequency and amplitude effects on the wake of a plunging airfoil*, AIAA Journal, 42 (10), 2042-2052, 2004.